Chemical Engineering Journal 157 (2010) 131–139

Contents lists available at ScienceDirect

Chemical Engineering Journal

journal homepage: www.elsevier.com/locate/cej

# Evaluation of rate of cyclopentane hydrate formation in an oscillatory baffled column using laser induced fluorescence and energy balance

C.J. Brown, X. Ni*

*Centre for Oscillatory Baffled Reactor Applications (COBRA), School of Engineering and Physical Science, Heriot-Watt University, Riccarton, Edinburgh EH14 4AS, UK*

ARTICLE INFO

*Article history:*
Received 2 July 2009
Received in revised form 2 November 2009
Accepted 13 November 2009

*Keywords:*
Oscillatory baffled column
Laser induced fluorescence
Cyclopentane
Gas hydrates
Hydrate formation
Energy balance

ABSTRACT

We report a novel method using laser induced fluorescence (LIF) for observing cyclopentane hydrate formation in an oscillatory baffled column (OBC). In LIF, a dye fluoresces in a hydrate system when induced by a laser; this highlights the areas in which hydrates are present, allowing the hydrate formation regimes to be identified and rates evaluated. Using temperature measurements of the system, the rates of hydrate formation are also determined by a thermal method. The work shows that there is a high correlation between the LIF and the thermal techniques in obtaining kinetic information on cyclopentane hydrate. The results indicate that there are possibly three mechanisms governing hydrate growth. With the absence of mixing, a film formation is observed. At high mixing intensities uniform droplet dispersion is resulted, where fluid mechanics is the controlling parameter. At low mixing conditions a combination of the two mechanisms co-exists, interfacial mechanics is thought to be the dominant factor. The trends in the rates of hydrate formation are different in each of these regimes.



## 1. Introduction

When pressurised, cooled and mixed with a range of (guest) molecules, from hydrocarbon gases (methane, ethane and propane) to water soluble and insoluble solvents (tetrahydrofuran and cyclopentane) as well as some non-hydrocarbon gases (carbon dioxide and hydrogen), water will form crystalline compounds known as clathrate hydrates. Through hydrogen bonding the water (host) molecules arrange into a framework containing large cavities that can be occupied by the guest molecules. These structures are similar to crystal framework formed by freezing pure water to ice, however, due to non-bonded interactions between the encaged guest molecules and the water cavities, these clathrate hydrates are thermodynamically stable at conditions typically unsuitable for ice [1], e.g. at atmospheric pressure ice melts at 273.2 K, whereas cyclopentane hydrates at 280.9 K [1]. Depending on the nature and size of the guest molecules, hydrates will form one of three structures: sI, small pentagonal dodecahedron and large tetrakaidecahedron cages [2]; sII, small pentagonal dodecahedron and large hexakaidecahedron cages [3] or sH, small pentagonal dodecahedron, medium irregular dodecahedron and large icosahedron cages [4].

In seeking to discover more about the equilibrium and kinetics of hydrates, numerous techniques have been employed ranging from rheometery [5], differential scanning calorimetry [6,7], scanning electron microscopy [8] and neutron spectroscopy [9], to molecular scale measurements through scattering of X-rays [10] as well as Raman spectroscopy [11,12]. At macroscopic level, particle video microscopy [13] and infrared imaging [14] have also been utilised to obtain information relating to fluid mechanical conditions under which hydrates are formed. However, to date no work has been published regarding the use of laser induced fluorescence (LIF).

LIF is a spectroscopy technique employed in studies of flow visualisation and measurement. Areas of applications can be found from combustion of gases and liquids [15,16], human and cell biology [17,18] to reaction kinetics and energy transitions [19–21]. LIF relies on the absorption, excitation and emission (fluorescence) of energy from certain molecules, generally a special dye. When illuminated with laser light of a certain wavelength (high energy photons), e.g. 510 nm, the molecules are promoted to a higher energy state (excitation). However, these higher energy states are unstable and quickly decay back to the lower one. During this decay photons of a lower energy than the ones applied are emitted at a higher wavelength, e.g. 590 nm. This can be utilised by recording the light emission using a digital camera coupled with a filter to only accommodate light of the higher wavelength. In this way, an image recording of such a light emission due to fluorescence can be obtained; in turn this is closely related to the physical or chemical changes of the focused element occurring in a system.

Although numerous models exist for the nucleation and growth of clathrate hydrates the majority of models are based on mass transfer being the limiting factor [1]. Therefore, a reactor that

* Corresponding author. Tel.: +44 1314513781; fax: +44 1314513129.
*E-mail address:* x.ni@hw.ac.uk (X. Ni).

1385-8947/$ – see front matter © 2009 Elsevier B.V. All rights reserved.
doi:10.1016/j.cej.2009.11.019

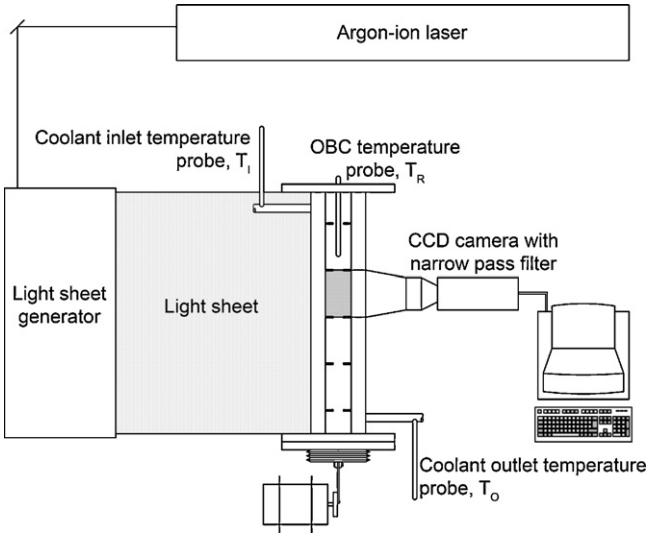


**Fig. 1.** Experimental setup (hatched area represents one baffled cell).

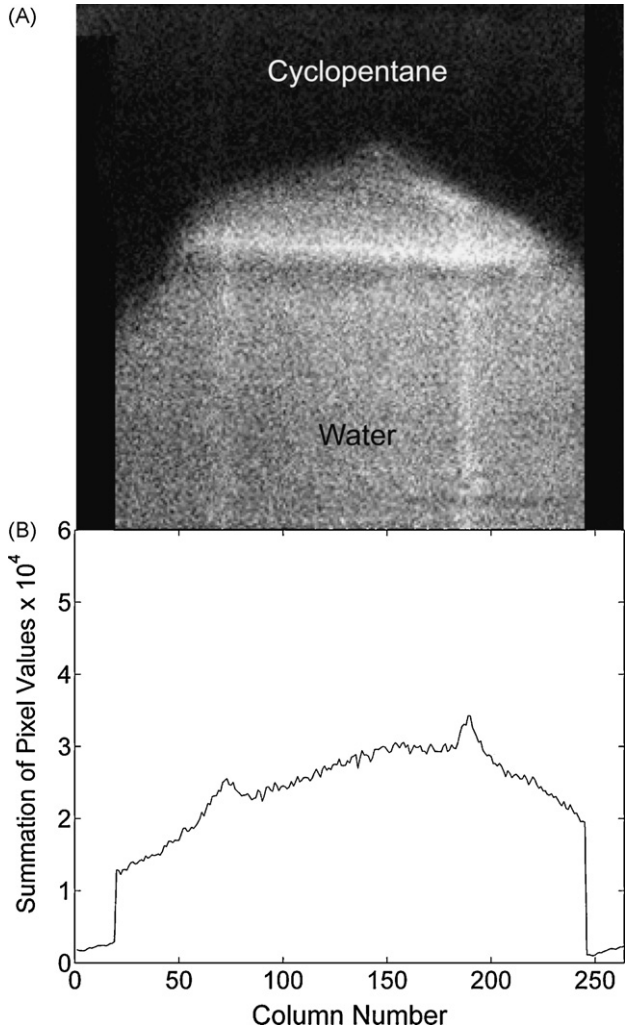


**Fig. 2.** (A) LIF image before hydrate formation and (B) the area plot for one image frame.

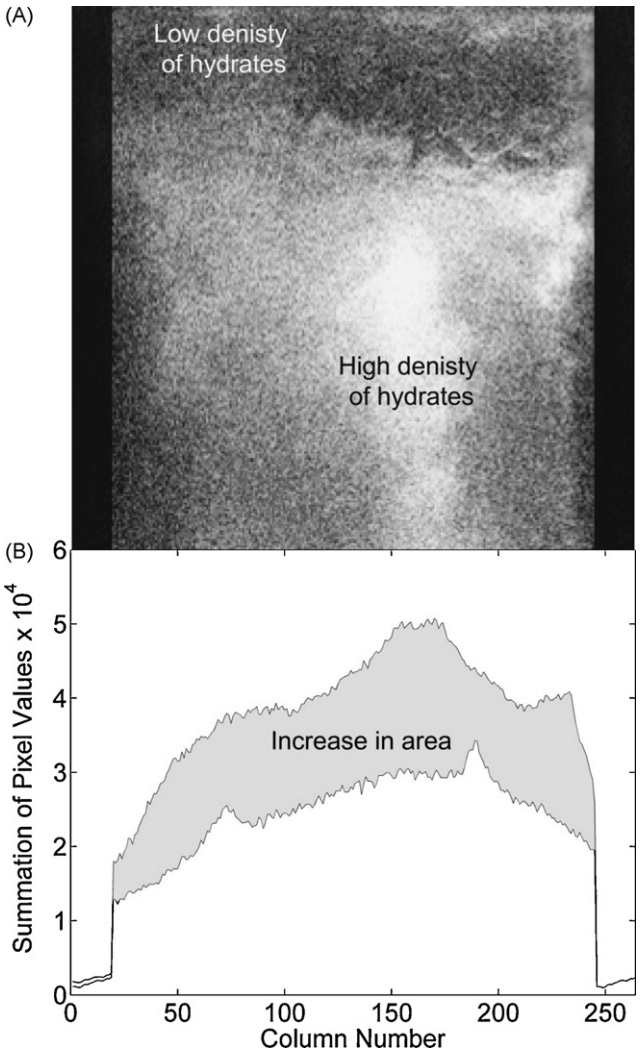


**Fig. 3.** (A) LIF image after hydrate formation and (B) a plot showing area difference.

enhances mass transfer rates would be desired, to this extent an oscillatory baffled column (OBC) was employed.

The mixing in OBC is achieved by eddies that are created when oscillatory motion of fluids pass through stationary orifice plates. Previous studies show that the mixing is uniform [22–25] and mass

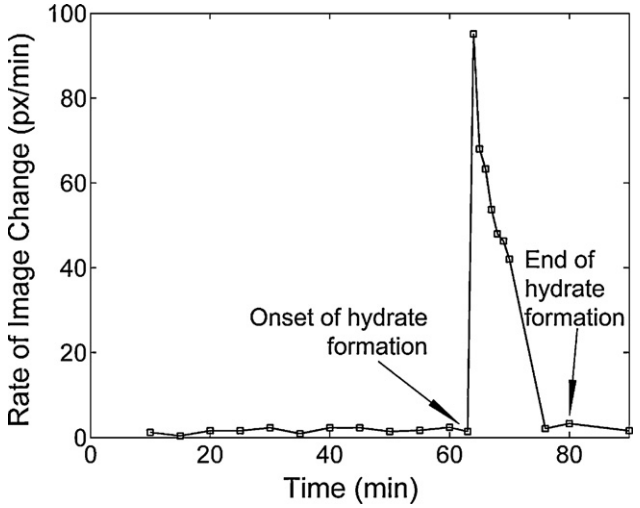


**Fig. 4.** Rate of image change as a function of time ($Re_o$ = 767, St = 0.637).

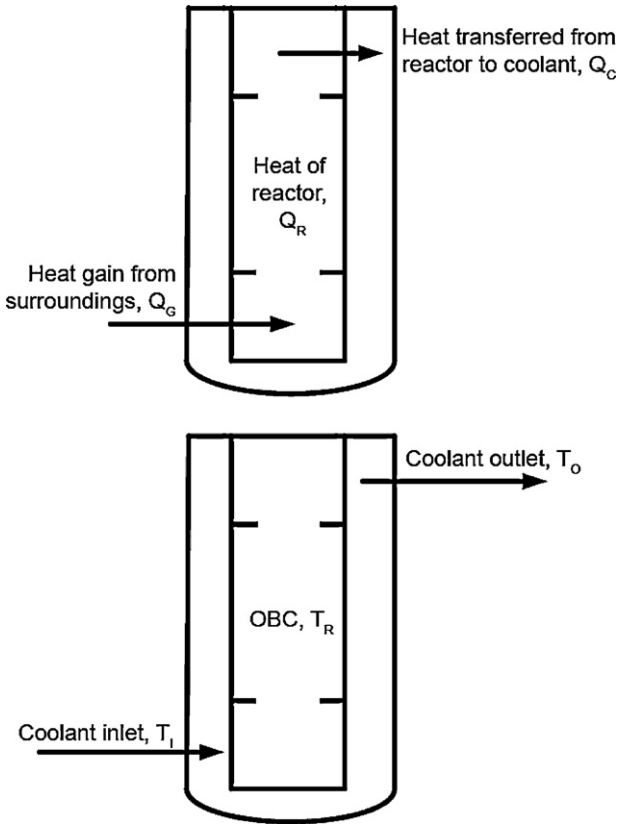


**Fig. 5.** Location of heat flows and temperature probes.

transfer is much higher than that in a conventional stirred tank [26]. Fluid mechanics of an OBC can be characterised by the dimensionless oscillatory Reynolds number ($Re_o$) and Strouhal (St) number, based on the amplitude of oscillation, $x_o$ (m), angular frequency, $\omega$ (rad/s), diameter of column, $D$ (m), kinematic viscosity of fluid, $\nu$ ($m^2/s$) as

$$Re_o = \frac{x_o \omega D}{\nu} \quad (1)$$

$$St = \frac{D}{4\pi\, x_o} \quad (2)$$

Cyclopentane–water hydrate was chosen as the model system for our work that is carried out in an OBC. The reasons of selecting cyclopentane–water system are:

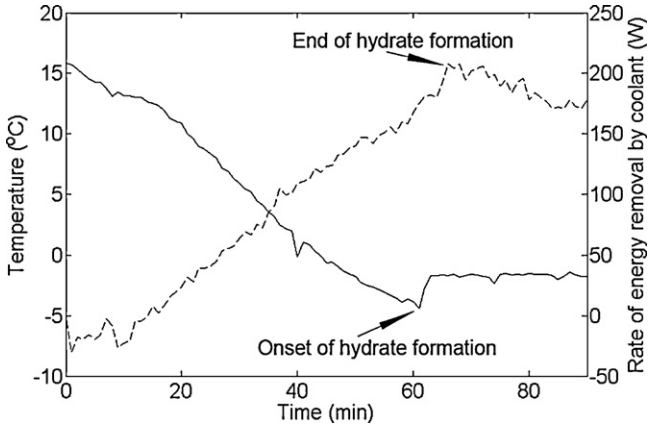


**Fig. 6.** Temperature and rate of energy removal by coolant ($Q_C$) as a function of time ($Re_o$ = 767, St = 0.637).

(a) these are of liquid state, enabling hydrate formation at relatively mild conditions;
(b) the pressure changes are minimal allowing optic techniques, such as LIF, to be implemented;
(c) the cyclopentane–water hydrate is of the sII type, which is the most commonly found structure in the oil and gas industry [6];
(d) a significant amount of work has already been carried out using cyclopentane–water hydrates, advocating their use as a suitable laboratory analogy [6,27,28].

For the sII hydrates aforementioned, the largest water cavity has a radius of 4.73 Å. In LIF, we add a fluorescent dye in water, the size of dye molecule is much larger than that of the cavity. This means that the dye molecule will not enter the cavities, but highlight the areas where activities of hydrates are not or less present. By analysing the fluorescence patterns, the amount of hydrate produced can indirectly be determined. This is the base for us to adopt LIF in the hydrate study. Incidentally, the smaller unfilled cavities in the cyclopentane–water hydrate could be filled by other gas guest molecules at moderate conditions [6], this would extend the application of LIF technique to the study of hydrate further far a field.

## 2. Experimental setup, operational and analytical procedures

An OBC and LIF that are similar to a previous study [29] are used, the schematic of which is shown in Fig. 1. Light was supplied by a continuous 4 W Argon-Ion laser (Spectra Physics) and a light sheet generator, consisting of a combination of a 16-sided rotating mirror and a parabolic mirror. This 1 mm wide light sheet was directed through the centre of the OBC that is operated vertically. A neutrally buoyant dye, Rhodamine B, was utilised as the fluorescence agent.

The OBC consisted of a square jacketed column with 5 equal spaced stationary orifice baffles (the provision of the square jacket is to minimise the curvature effect when using optic equipment, such as LIF). Fluid oscillation was applied via a diaphragm driven by an electric motor. Temperature probes were installed along the column to monitor the profile within the OBC, as well as that of coolant inlet and outlets. Temperatures were recorded via a data logging software (LoggerPro) installed on a PC. The detailed setup can be found elsewhere [29].

The OBC was filled with 145 ml of water, 40 ml of cyclopentane ($C_5H_{10}{\cdot}19H_2O$) together with 10 ml Rhodamine B dye equalling to $0.322 \times 10^{-7}$ mol/l [30]. The dye is soluble and neutrally buoyant in water, but insoluble in cyclopentane. Oscillation was applied to the OBC at 5 Hz and 4 mm for 5 min in order to fully disperse the dye into water. The solution was then left for 30 min to allow the cyclopentane and water phases to separate out. Prior to imaging, there is a clear interface between cyclopentane and water/dye solution, with cyclopentane being less dense at the top, as shown in Fig. 2A. The OBC is now cooled and maintained at 263.2 K by pumping ethylene glycol/water coolant at 258.2 K to the shell side of the OBC at 8.3 ml/s, subsequently cyclopentane hydrate is induced and formed. At the same time the OBC was oscillated at 2 Hz and 4 mm in order to promote uniform mixing. Temperature logging was taken at a rate of 1 reading every 10 s from the start.

In parallel to the operation of the OBC the column was illuminated by a light sheet of 1 mm by 300 mm at its maximum exposure time of 0.5 ns. An image set, consisting of 50 frames, was taken using a CCD camera (SensiCam) fitted with a narrow pass filter (590 nm) at an initial interval of every 5 min, followed by every 1 min during the formation of hydrate. Each image set was then loaded into Matlab for further processing. Images were converted to greyscale where each pixel can have a value rang-

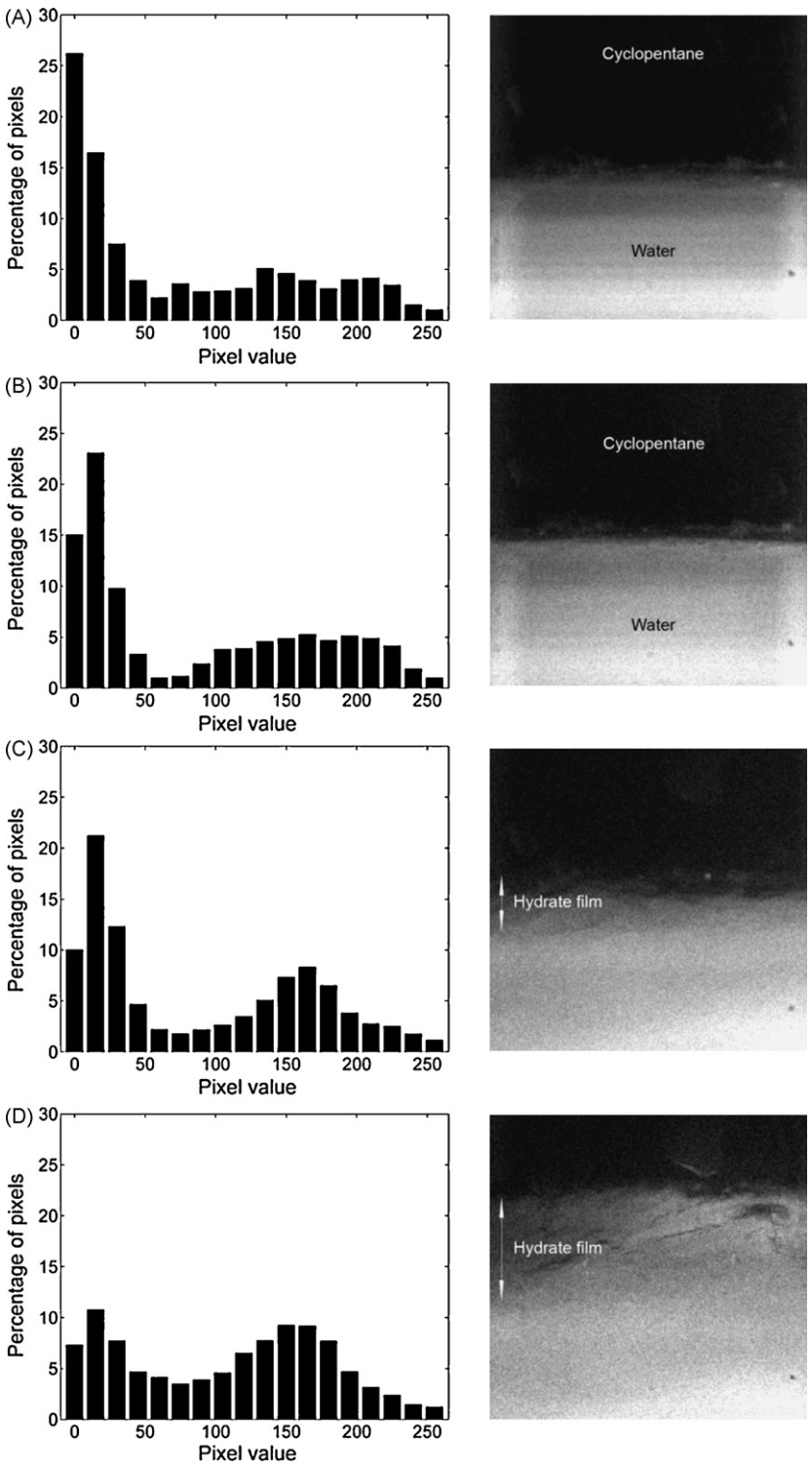


**Fig. 7.** Histograms for $Re_o = 0$ at initial conditions (A), pre-hydrate formation (B), post-hydrate formation (C) and final conditions (D).

ing from 0 (black) to 255 (white). At the start pixels with a high value represent water with the presence of fluorescent dye in white colour, whereas pixels with a low value indicate cyclopentane in black colour, as shown in Fig. 2A. For each individual frame, it is divided into many pixels, each column of pixels was then summated and plotted against the corresponding column number [30], as shown in Fig. 2B. Since the summation of the pixels is related to the distribution and variation of dye in the system, the area under the curve would correspond to the area of the image with the presence of dye. This area was calculated via the trapezoid rule.

The area of the image affected by dye was then averaged over the 50 frames for that image set. This minimised any effect of fluctuations in the image due to the oscillation on the calculated area. Standard deviation was also calculated as an indication of to what a degree the frames varied.

During the formation of hydrate the image in terms of pixel values is altered by the presence of hydrate crystals. Although the dye

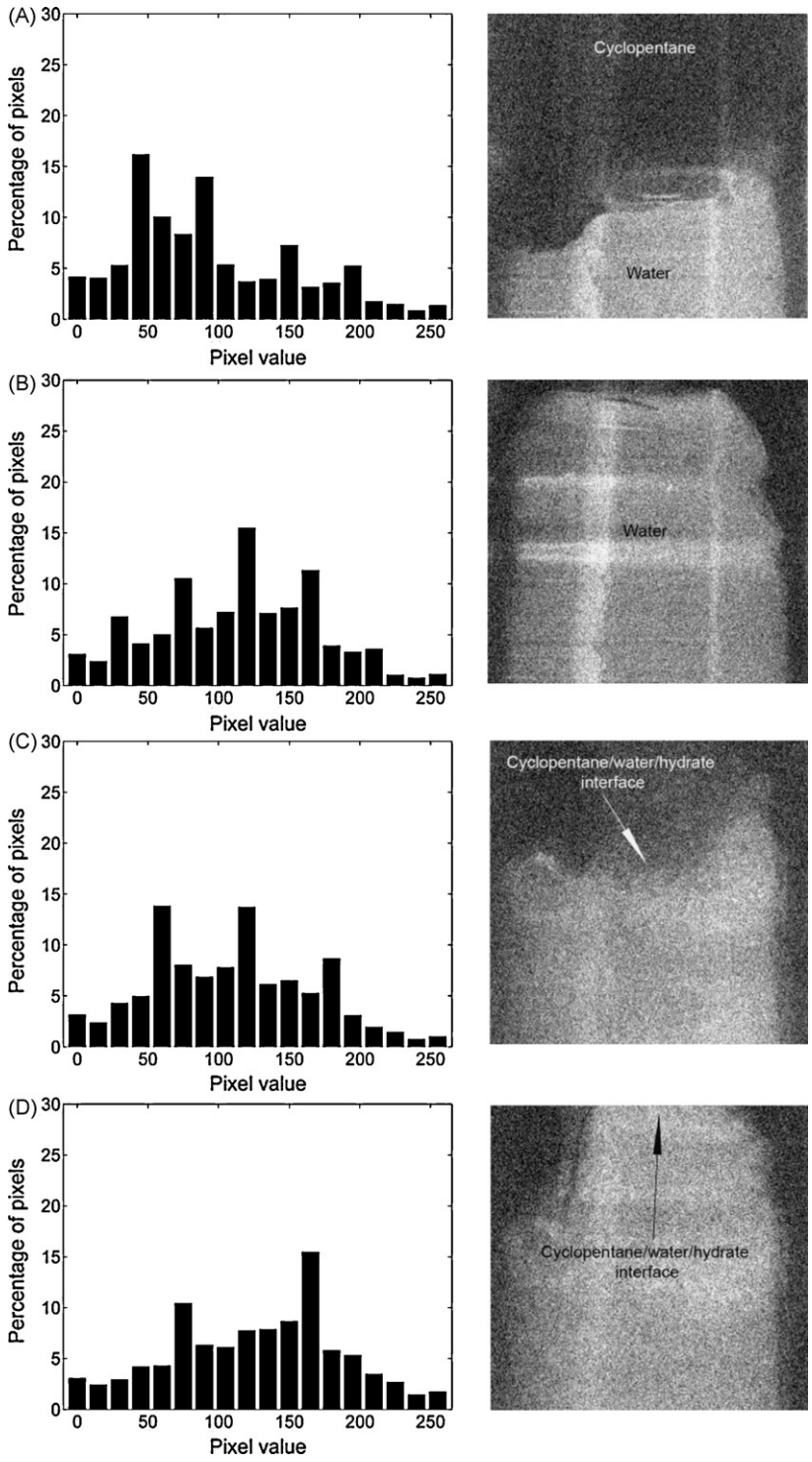


**Fig. 8.** Histograms for $Re_o$ = 767 at pre-hydrate formation (A) at the trough of an oscillation, pre-hydrate formation (B) at the peak of an oscillation, post-hydrate formation at the trough (C) and post-hydrate formation (D) at the peak.

molecules are too large in size to enter the hydrate cages, they can still be entrained between the hydrate crystals distributing the dye into the cyclopentane phase. Therefore, as hydrates form the percentage of white pixels would increase. As a result the summation of each column will increase in terms of pixel values.

In comparison of the areas affected by dye between with (the upper curve) and without (the lower curve) hydrates in Fig. 3B, the difference in the area (shaded) is closely associated with the amount of hydrate formed. It is the area difference that is used to determine the quantity of hydrates that have been produced in this study. Furthermore the net change in the area of white pixels divided by the time interval at which the change took place will give the rate of image change in pixel/min, which is related to the rate of hydrate generation. Plotting this rate against time in Fig. 4, we see a sharp rise during the hydrate formation by this method, which is followed by a steep decrease once the maximum quantity of hydrates has been produced. Note that this rate of change was determined over a complete run, with each point representing

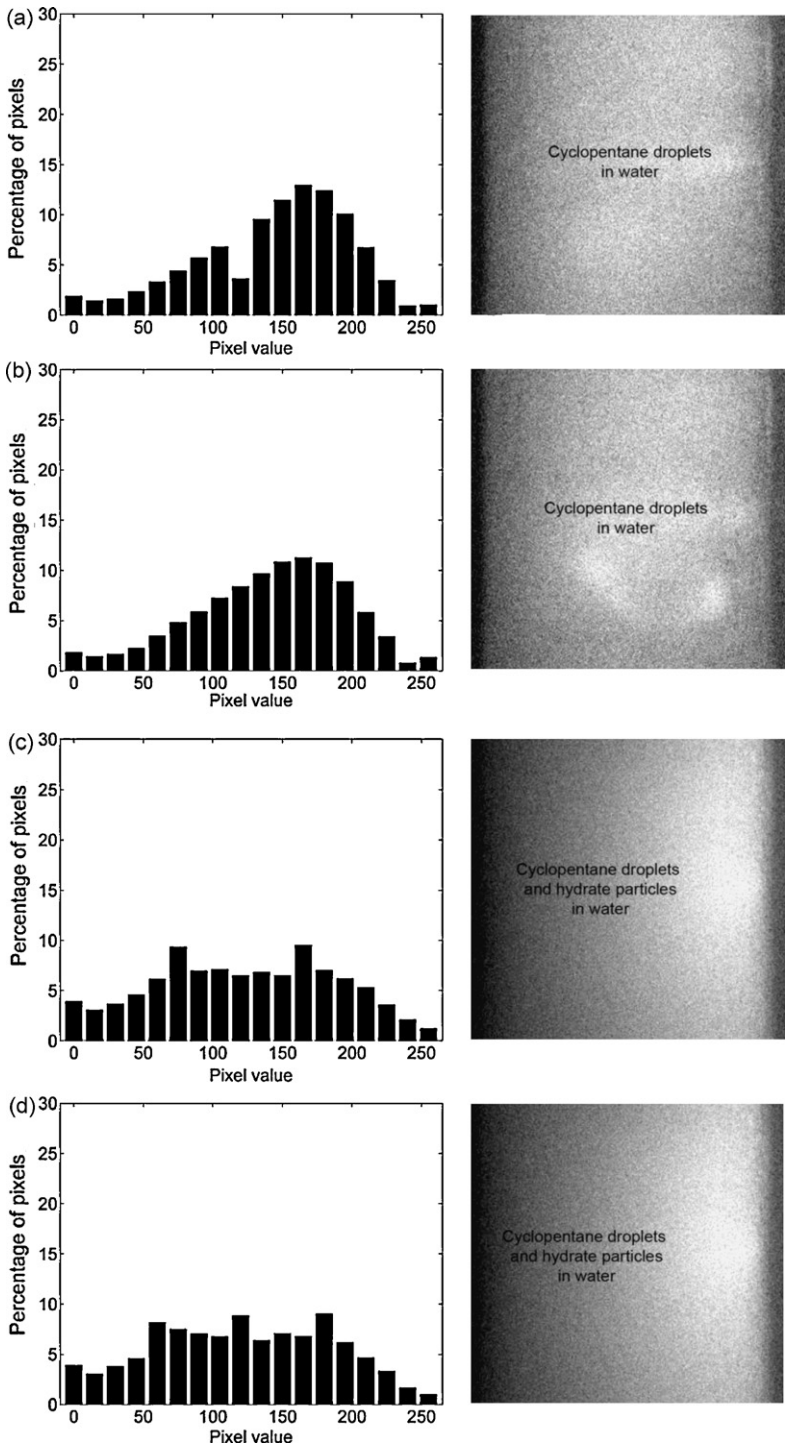


**Fig. 9.** Histograms for $Re_o$ = 1278 at pre-hydrate formation (A) at the trough of an oscillation, pre-hydrate formation (B) at the peak of an oscillation, post-hydrate formation at the trough (C) and post-hydrate formation (D) at the peak.

one image set consisting of 50 frames. It can be seen that the difference in the rate of image change between each image set from 10 to 62 min is initially minimal, suggesting that there was no or little activity of hydrate forming. A sudden surge occurred at about 63 min, indicating the start of hydrate formation. As the hydrate formation progressed further the changes in the rate lessened, until it levelled off from 76 min. The time at which the hydrate formation began was defined as the time when the largest positive change in the pixel rate (pixel/min) occurred, i.e. 63 min in Fig. 4. The end time of the hydrate formation was when the smallest change in the pixel rate took place, i.e. 80 min shown in Fig. 4. Therefore, the difference in these two points can be equated to the time taken to produce the corresponding amount of hydrates. For the sample size used in our work, a maximum of 206 g of hydrate was produced between 63 and 80 min, giving the overall averaged rate of hydrate generation is 12.2 g/min during this period.

## 3. Thermal analysis

To validate the hydrate formation rates evaluated from the LIF image analysis, the onset of hydrate formation can also be estimated through an energy balance around the system. To achieve

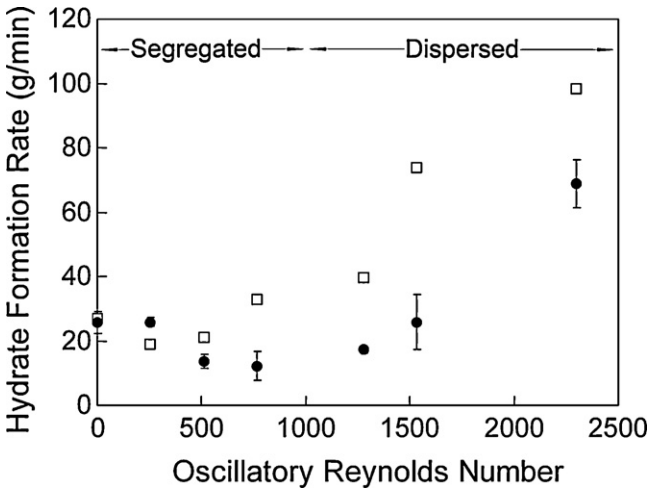


**Fig. 10.** Rate of hydrate formation as a function of oscillatory Reynolds number (□, thermal analysis; ●, image analysis).

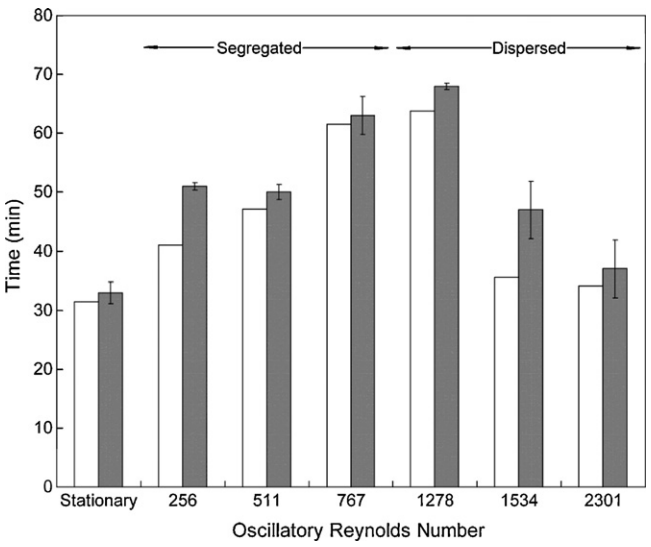


**Fig. 11.** Effect of mixing on the time required for hydrate formation (□, thermal analysis; ▓, image analysis).

this, temperatures of the coolant inlet, outlet and OBC must be known.

In Fig. 5, $Q_R$ is defined as the rate of energy change within the OBC. $Q_C$ and $Q_G$ are the rate at which energy is removed from the OBC by the coolant and gained by the OBC from the surrounding environment, respectively. Therefore, the total energy removed from the OBC is

$$-Q_R - Q_C + Q_G = 0 \quad (3)$$

$Q_G$ can be calculated from the differences in temperature between the coolant inlet and outlet with no formation of hydrate, i.e. this is the rate of energy gained by the OBC from the environment. Based on natural convection principles [31] and previous work with the OBC $Q_G$ was found to be on average 41 W. $Q_C$ can be calculated from the differences in the temperatures of coolant inlet and outlet when hydrate does occur.

Assuming the rate of heat gain from the environment ($Q_G$) was constant throughout each experiment, any variation in $Q_C$ would be attributed by the energy changes within the reactor, $Q_R$. Two energy sources are encountered for $Q_R$, firstly the sensible heat causing the temperature of the reactor, $T_R$, to decrease, secondly the latent heat relating to the formation of hydrate crystals causing the temperature of the reactor, $T_R$, to increase.

Shown in Fig. 6 are examples of the temperature and energy profiles. It can be seen that the temperature (solid line) of the reactor continually decreases until the point at which hydrate formation occurs, this corresponds to the sharp rise in temperature at 61 min due to the exothermic nature of this hydrate formation process. However, the reactor temperature remains constant from this point onwards, giving no indication of when the hydrate formation would have been completed. In terms of energy profile, on the other hand, the coolant energy curve (dashed line) shows a constant increase in the rate of energy ($Q_C$) removed from the reactor until 67 min and then a decrease. This would mark the end of hydrate formation as no more latent heat is contributing to the energy gain of the coolant. Similarly to the technique discussed in this section, the difference between these two points would give rise of the time period during which the hydrate formation had occurred, e.g. for the sample size used in our work 206 g of hydrate was produced between 61 and 67 min. Thus the overall averaged rate of hydrate generation is 34.3 g/min during this period.

## 4. Results and discussion

From visual inspection of the images captured, three distinct regimes of hydrate formation were observed. Firstly a hydrate film was formed at the interface between cyclopentane and water when no mixing was applied, then propagated into the cyclopentane phase with the march of time, as shown in Fig. 7.

The initial image in Fig. 7A highlights a stationary interface between cyclopentane and water with the corresponding histogram displaying a large percentage of black pixels (lower values) and a fairly even distribution of grey to white pixels (middle to high values). The image obtained prior to the onset of hydrate formation (Fig. 7B) is very similar in the distribution of pixel values to that of the starting position (Fig. 7A). Due to the interfacial phenomena [32,33], hydrate formation began at the interface, we see that the interface has moved vertically into the cyclopentane phase (Fig. 7C). In terms of the histogram, these interface movements correspond to a decrease in the percentage of black pixels and at the same time an increase in the percentage of white pixels, in comparison to those of the previous images in Fig. 7A and B. The image acquired some time after hydrate formation (Fig. 7D) shows additional evidence of the upwards interface movement, a further decrease in the percentage of black pixels together with an increase in the percentage of grey to white pixels. Once a hydrate layer has been formed at the interface, this reduces the rate of mass transfer between the two liquids [32] due to the increase of the thickness of the interface and perhaps more importantly the non-permeability of the hydrate layers [33].

Secondly a distinct interface between cyclopentane and water is visible at low mixing conditions, e.g. $Re_o = 767$, prior to the hydrate formation, and moves in synchronisation with oscillation, in this case, towards the trough of the oscillation cycle (Fig. 8A). Similar to the case with no oscillation the image translates into a certain percentage of black pixels (low value). Near the peak of the oscillation cycle, the interface is seen at the top of the baffled cell as shown in Fig. 8B with more white pixels in the image, this has shifted the peak of the distribution of the pixel value towards high values (to the right). Fig. 8C and D shows the interface after the hydrate formation within the full span of an oscillation cycle. From the images, there are more grey to white pixels towards both the trough (Fig. 8C) and the peak (Fig. 8D) of oscillation. The shapes of the pixel distributions have not altered significantly from their

**Table 1**
Hydrate formation rates.

| Formation rate (g/min) | Type | Size | Guest Molecule | Source |
|---|---|---|---|---|
| 0.0735 | Stirred tank (750 rpm) | 600 ml | Propane | [37] |
| 1.504 | Bubble column | Gas flux $2.5 \times 10^{-5}$ $m^3$/min | Methane | [36] |
| 2.64 | Stirred tank (350 rpm) | Unknown | $CO_2$ | [35] |
| 3.74 | Stirred tank (400 rpm) | Unknown | $CO_2$ | [35] |
| 5.21 | Stirred tank (450 rpm) | Unknown | $CO_2$ | [35] |
| 5.88 | Stirred tank (750 rpm) | 600 ml | $CO_2$ | [38] |
| 5.97 | Stirred tank (500 rpm) | Unknown | $CO_2$ | [35] |
| 10.53 | Bubble column | Gas flux $25 \times 10^{-5}$ $m^3$/min | Methane | [36] |
| 18.8 | $Re_o = 256$ | 200 ml | C-pentane | Our work |
| 21.0 | $Re_o = 511$ | 200 ml | C-pentane | Our work |
| 32.8 | $Re_o = 767$ | 200 ml | C-pentane | Our work |
| 39.7 | $Re_o = 1278$ | 200 ml | C-pentane | Our work |
| 73.8 | $Re_o = 1534$ | 200 ml | C-pentane | Our work |
| 98.4 | $Re_o = 2301$ | 200 ml | C-pentane | Our work |

non-hydrate counter parts (Fig. 8A and B), but the distribution is flatter with a shift towards higher values.

Finally Fig. 9 captured the images of hydrate formation at well mixed conditions, in this case, $Re_o = 1278$. As expected the images show uniform mixing of the two phases before the start of hydrate formation, and there is very little difference in the pixel distribution near the trough (Fig. 9A) and peak (Fig. 9B) of an oscillation cycle. Likewise similar images can be seen after the formation of hydrate for both the trough (Fig. 9C) and peak (Fig. 9D) of an oscillation cycle. The histogram gives a flatter and more even distribution of pixels compared to the non-hydrate benchmark.

In summary, the formation of a hydrate film was observed at stationary condition, similar to those noted by Taylor et al. [32] and Tohidi et al. [33]. When thorough mixing was applied ($Re_o > 1000$) cyclopentane droplets were formed and disturbed evenly into the water phase, leading to the formation of hydrate particles that was reported by Nakajima et al. [34]. However, low mixing conditions ($Re_o < 1000$) did not deliver uniform cyclopentane droplets in the system, nor did the existence of a stable film. As a consequence of this, a combination of two mechanisms co-existed under those conditions.

Incidentally the identification of the three regimes of hydrate formation in this work highlights much wider implications and benefits to be gained by using the LIF method in observing mixing regimes in any chemical and biochemical system.

Fig. 10 plots the rate of hydrate formation evaluated using the two methods vs. the oscillatory Reynolds number. It can be seen that the mean overall rate of hydrate formation decreases with the increase of $Re_o$ initially, and then rises with any further increase of $Re_o$. The display of such a trend would coincide with the change in the mechanism of hydrate formation before and after a critical mixing intensity as we discussed earlier.

Under uniform mixed conditions ($Re_o > 1000$), a well dispersed phase of cyclopentane in water has been formed, this provides much increased surface area for mass transfer. As the direct result of this, an increase in the rate of hydrate formation is expected and observed. A similar trend was noted by Clarke and Bishnoi [35], where an increase in the stirring speed of their stirred tank reactor led to an increase in the hydrate formation rate. Luo et al. [36] also reported an increase in the rate of hydrate formation with an increase in gas flux in their bubble column system. Our finding is consistent with these pre-arts.

The rate of hydrate formation decreased with the increase of the oscillatory Reynolds numbers at low $Re_o$ (<1000), this is likely due to the co-existence as well as the competition of the two mechanisms in the system, as we discussed earlier in the text. Further evidence in the times recorded before the formation of hydrate as shown in Fig. 11 supports our discussions. Clearly the times required for the start of hydrate formation are delayed or longer when two mechanisms occupy the same space, leading to lower rates evaluated.

In terms of the two techniques used in this work, although there is a high correlation between the trends observed, there are marked differences in the actual values. These are likely due to the detection rate between a thermocouple and a CCD camera. The data of temperature change was collected at a rate of 1 data every 10 s, while the rate of the CCD camera was averaged to 1 shot every 60 s. This would mean that some activities and interactions of hydrate formation are too small or too fast to be detected by the camera, leading to smaller rates of hydrate formation by the LIF technique than that by the thermal method. With better camera and larger digital storage space, we believe that these differences in the rates evaluated would decrease accordingly.

In order to compare to our findings with other studies, Table 1 compiles the rate of hydrate formation from recent work. It should be noted that there are currently no data available on liquid guest molecules and all the previous work listed in Table 1 involved gas guest molecules, where these must be dissolved into the water first prior to the formation of hydrate; this adds to additional barrier for mass transfer. Not surprisingly, the rates determined by our study are at least one order of magnitude higher than the rest; only Luo et al. [36] achieved a similar rate. In that case, the reactor consisted of a water column with the presence of fine or mist of bubbles. Due to the limited data, this comparison would serve as merely an indication.

## 5. Conclusions

We reported that the rate and mechanism of hydrate formation in cyclopentane–water system can be determined and observed using non-intrusive laser induced fluorescence technique, these results are validated by an independent technique. Three formation mechanisms are proposed: for a stationary condition the formation of a hydrate film was the governing interfacial mechanism for the generation of hydrate. At well mixed conditions, the cyclopentane was well dispersed as droplets into the water phase, the formation of hydrate particles was regulated by fluid mechanics within the OBC. At low mixing conditions a combination of interface and droplet dispersion was co-present, the rate of which was lower than that with one dominant mechanism of hydrate formation. This work clearly demonstrated the ability and capability of the LIF technique as a useful tool in quantifying hydrate formation as well as identifying mixing regimes in any chemical and biochemical reactor.

## Acknowledgement

The authors wish to thank Heriot-Watt University for the research scholarship, allowing this work to be possible.

## References


[1] E.D. Sloan, C.A. Koh, Clathrate Hydrates of Natural Gases, vol. 3, CRC Press, 2007.
[2] R.K. McMullan, G.A. Jeffrey, Polyhedral clathrate hydrates. IX. Structure of ethylene oxide hydrate, The Journal of Chemical Physics 42 (1965) 2725–2732.
[3] T.C.W. Mak, R.K. McMullan, Polyhedral clathrate hydrates. X. Structure of the double hydrate of tetrahydrofuran and hydrogen sulfide, The Journal of Chemical Physics 42 (1965) 2732–2737.
[4] J.A. Ripmeester, J.S. Tse, C.I. Ratcliffe, B.M. Powell, A new clathrate hydrate structure, Nature 325 (1987) 135–136.
[5] R. Camargo, T. Palermo, A. Sinquin, P. Glenat, Rheological characterization of hydrate suspensions in oil dominated systems, Gas Hydrates: Challenges for the Future 912 (2000) 906–916.
[6] Y. Zhang, P.G. Debenedetti, R.K. Prud'homme, B.A. Pethica, Differential scanning calorimetry studies of clathrate hydrate formation, Journal of Physical Chemistry B 108 (2004) 16717–16722.
[7] P. Le Parlouer, C. Dalmazzone, B. Herzhaft, L. Rousseau, C. Mathonat, Characterisation of gas hydrates formation using a new high pressure MICRO-DSC, Journal of Thermal Analysis and Calorimetry 78 (2004) 165–172.
[8] A. Falenty, G. Genov, W.F. Kuhs, From ice to $CO_2$ hydrates and back—study of nucleation and initial growth using scanning electron microscopy, in: Proceedings of the 11th International Conference on the Physics and Chemistry of Ice, Bremerhaven, 2007.
[9] J.S. Tse, C.I. Ratcliffe, B.M. Powell, V.F. Sears, Y.P. Handa, Rotational and translational motions of trapped methane. Incoherent inelastic neutron scattering of methane hydrate, Journal of Physical Chemistry A 101 (1997) 4491–4495.
[10] C.C. Tang, C.A. Koh, A.A. Neild, R.J. Cernik, R.E. Motie, R.I. Nooney, J.L. Savidge, High-pressure cell for the study of in situ hydrates using energy-dispersive X-ray diffraction, Journal of Synchrotron Radiation 3 (1996) 220–224.
[11] A.K. Sum, R.C. Burruss, E.D. Sloan, Measurement of clathrate hydrates via Raman spectroscopy, Journal of Physical Chemistry B 101 (1997) 7371–7377.
[12] V. Thieu, S. Subramanian, S.O. Colgate, E.D. Sloan, High-pressure optical cell for hydrate measurements using Raman spectroscopy, Gas Hydrates: Challenges for the Future 912 (2000) 983–992.
[13] D. Greaves, J. Boxall, J. Mulligan, A. Montesi, J. Creek, E.D. Sloan, C.A. Koh, Measuring the particle size of a known distribution using the focused beam reflectance measurement technique, Chemical Engineering Science 63 (2008) 5410–5419.
[14] P. Long, Phase II core handling and core analysis–IR imaging of cores, Chevron-Texaco JIP workshop, Winchester, 2003.
[15] D.S. Shringi, B.D. Shaw, H.A. Dwyer, Laser-induced fluorescence imaging of acetone inside evaporating and burning fuel droplets, Optics and Lasers in Engineering 47 (2009) 51–56.
[16] U. Stopper, M. Aigner, W. Meier, R. Sadanandan, M. Stohr, I.S. Kim, Flow field and combustion characterization of premixed gas turbine flames by planar laser techniques, in: 53rd ASME Turbo Expo, Berlin, Germany, 2008.
[17] S. Cho, S.C. Ji, S. Hur, J. Bae, I.S. Park, Y.C. Song, Optimum temperature and salinity conditions for growth of green algae *Chlorella ellipsoidea* and *Nannochloris oculata*, Fish Science 73 (2007) 1050–1056.
[18] Y.-H. Deng, H. Wang, L. Zhong, H.-S. Zhang, Trace determination of short-chain aliphatic amines in biological samples by micellar electrokinetic capillary chromatography with laser-induced fluorescence detection, Talanta 77 (2009) 1337–1342.
[19] O. Gabriel, J.J.A. van den Dungen, E. Roueff, H. Abgrall, R. Engeln, Lyman transitions of high rovibrationally excited H-2, HD and D-2 molecules, Journal of Molecular Spectroscopy 253 (2009) 64–72.
[20] X. Huang, P. Terech, S.R. Raghavan, R.G. Weiss, Kinetics of 5a-cholestan-3-yl N-(2-naphthyl)carbamate/n-alkane organogel formation and its influence on the fibrillar networks, Journal of the American Chemical Society 127 (2005) 4336–4344.
[21] M. Nakajima, T.W. Schmidt, A. Miyoshi, Y. Sumiyoshi, Y. Endo, Gas-phase spectroscopy of the 2 (3)Sigma(−)-X (3)Sigma(−) electronic transition of CCS, Journal of Chemical Physics 130 (2009) 10.
[22] M.R. Mackley, X. Ni, Mixing and dispersion in a baffled tube for steady laminar and pulsatile flow, Chemical Engineering Science 46 (1991) 3139–3151.
[23] M.R. Mackley, X. Ni, Experimental fluid dispersion measurements in periodic baffled tube arrays, Chemical Engineering Science 48 (1993) 3293–3305.
[24] M.R. Mackley, P. Stonestreet, E.P.L. Roberts, X. Ni, Residence time distribution enhancement in reactors using oscillatory flow, Chemical Engineering Research & Design 74 (1996) 541–545.
[25] X.W. Ni, Residence time distribution measurements in a pulsed baffled tube bundle, Journal of Chemical Technology and Biotechnology 59 (1994) 213–221.
[26] X. Ni, S. Gao, R.H. Cumming, D.W. Pritchard, A comparative-study of mass-transfer in yeast for a batch pulsed baffled bioreactor and a stirred-tank fermenter, Chemical Engineering Science 50 (1995) 2127–2136.
[27] C.A. Whitman, R. Mysyk, M.A. White, Investigation of factors affecting crystallization of cyclopentane clathrate hydrate, Journal of Chemical Physics 129 (2008) 6.
[28] Z.G. Sun, S.S. Fan, K.H. Guo, L. Shi, Y.K. Guo, R.Z. Wang, Gas hydrate phase equilibrium data of cyclohexane and cyclopentane, Journal of Chemical and Engineering Data 47 (2002) 313–315.
[29] A.W. Fitch, X. Ni, On the determination of axial dispersion coefficient in a batch oscillatory baffled column using laser induced fluorescence, Chemical Engineering Journal 92 (2003) 243–253.
[30] H. Golnabi, Precise CCD image analysis for planar laser-induced fluorescence experiments, Optics and Laser Technology 38 (2006) 152–161.
[31] J.M. Coulson, J.F. Richardson, J.R. Backhurst, J.H. Harker, Fluid Flow, Heat Transfer and Mass Transfer, Butterworth-Heinemann, Oxford, UK, 1999.
[32] C.J. Taylor, K.T. Miller, C.A. Koh, E.D. Sloan, Macroscopic investigation of hydrate film growth at the hydrocarbon/water interface, Chemical Engineering Science 62 (2007) 6524–6533.
[33] B. Tohidi, R. Anderson, M.B. Clennell, R.W. Burgass, A.B. Biderkab, Visual observation of gas-hydrate formation and dissociation in synthetic porous media by means of glass micromodels, Geology 29 (2001) 867–870.
[34] M. Nakajima, R. Ohmura, Y.H. Mori, Clathrate hydrate formation from cyclopentane-in-water emulsions, Industrial & Engineering Chemistry Research 47 (2008) 8933–8939.
[35] M.A. Clarke, P.R. Bishnoi, Determination of the intrinsic kinetics of $CO_2$ gas hydrate formation using in situ particle size analysis, Chemical Engineering Science 60 (2005) 695–709.
[36] Y.T. Luo, J.H. Zhu, S.S. Fan, G.J. Chen, Study in the kinetics of hydrate formation in a bubble column, Chemical Engineering Science 62 (2007) 1000–1009.
[37] S. Bergeron, P. Servio, Reaction rate constant of propane hydrate formation, Fluid Phase Equilibria 265 (2008) 30–36.
[38] S. Bergeron, P. Servio, Reaction rate constant of CO2 hydrate formation and verification of old premises pertaining to hydrate growth kinetics, AIChe Journal 54 (2008) 2964–2970.